



ELSEVIER

Contents lists available at ScienceDirect

Inorganic Chemistry Communications

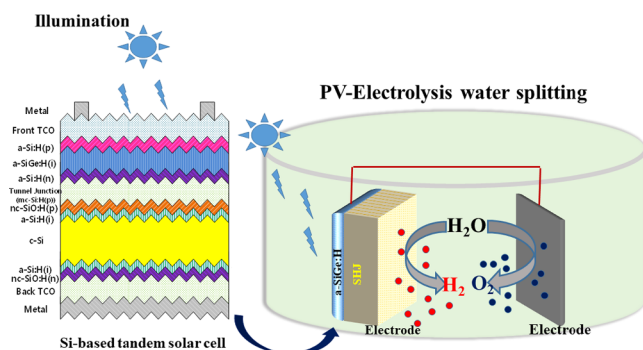
journal homepage: www.elsevier.com/locate/inoche

Monocrystalline silicon-based tandem configuration for solar-to-hydrogen conversion

Duy Phong Pham^a, Sunhwa Lee^a, Anh Huy Tuan Le^{b,c}, Eun-Chel Cho^a, Young Hyun Cho^{a,*}, Junsin Yi^{a,*}^a College of Information and Communication Engineering, Sungkyunkwan University, Suwon 440-746, Republic of Korea^b Division of Computational Physics, Institute for Computational Science, Ton Duc Thang University, Ho Chi Minh City, Viet Nam^c Faculty of Electrical and Electronics Engineering, Ton Duc Thang University, Ho Chi Minh City, Viet Nam

GRAPHICAL ABSTRACT

Schematic of the photovoltaic-electrolysis water splitting system using an a-SiGe/SHJ tandem solar cell as the source of electricity.



ARTICLE INFO

Keywords:

Solar-to-hydrogen production
 Photoelectrochemical water splitting
 a-SiGe:H thin film solar cells
 Tandem solar cells
 SHJ solar cells
 Photovoltaic-electrolysis system

ABSTRACT

Hydrogen gas produced from a photovoltaic power source for water electrolysis is a promising renewable, low-cost, storable, and transportable energy source. Herein, we propose a simply integrated hydrogenated amorphous silicon germanium (a-SiGe:H)/silicon heterojunction (SHJ) tandem configuration as an integrated photovoltaic-electrolysis device. By optimising the a-SiGe:H top cell for high efficiency using various band-gap engineering techniques, we achieve effective performance enhancement, with a maximum V_{oc} of greater than 1.5 V. Assuming an ideal condition wherein the photovoltaic device operates at maximum power and the output conversion performance is maximized, we estimate a solar-to-hydrogen (STH) conversion performance of 13.1%. The integrated a-SiGe:H/SHJ structure can generate a sufficiently high voltage for water electrolysis while using lesser silicon than single-junction silicon solar cells connected in series. Consequently, it is a viable option for a low-cost, high-efficiency integrated photovoltaic-electrolysis system and an alternative to traditional hydrogen production from fossil fuels.

Abbreviations: SHJ, silicon heterojunction; STH, solar-to-hydrogen; PV, photovoltaic; PEC-WS, photo-electro-chemical water splitting; CIGS, copper indium gallium selenide; PECVD, plasma enhanced chemical vapor deposition; FF, fill factor

* Corresponding authors.

E-mail addresses: pdphong@skku.edu (D.P. Pham), lehuytuananh@tdtu.edu.vn (A.H.T. Le), yhcho64@skku.edu (Y. Hyun Cho), junsin@skku.edu (J. Yi).<https://doi.org/10.1016/j.inoche.2020.107926>

Received 14 February 2020; Received in revised form 17 March 2020; Accepted 1 April 2020

Available online 01 April 2020

1387-7003/ © 2020 Elsevier B.V. All rights reserved.

1. Introduction

The effective use of the abundant solar energy available on Earth is a constantly evolving research field. In addition to production of electricity from sunlight using photovoltaic (PV) devices, the conversion of solar radiation into a storable and transportable fuel source can maximise solar energy use [1,2]. Since Fujishima and Honda were the first to attempt the photolysis of water using a titanium dioxide (TiO_2) photo-anode and a platinum (Pt) cathode [3], producing hydrogen fuel from photo-electro-chemical water splitting (PEC-WS) has emerged as a sustainable alternative to traditional hydrogen production from fossil fuels [4–6]. The PEC-WS process does not release carbon dioxide (CO_2), and is a clean and environmentally safe manufacturing process compared to traditional fossil fuel processes [7,8]. Several attempts have been made to produce hydrogen from water electrolysis, using various semiconductor materials [9] and approaches [10–12]. However, creating a low-cost high-efficiency PEC-WS system capable of competing with the traditional fossil fuel production system remains a challenge [13,14].

With the rapid development of photovoltaic devices, scientists have proposed an integrated PV and electrolysis water splitting (PV-EWS) device for hydrogen fuel production [12,14]. In these devices, solar cells provide the electricity required for water electrolysis. Typically, the water-splitting mechanism requires a minimum voltage of 1.23 V to overcome the energy barrier of the water decomposition reaction and to supply the thermodynamic driving force [12,13,15]. However, to fulfil the practical overpotential requirements of the electrocatalysts owing to reaction kinetics and other system losses, a larger applied photo-voltage of 1.5 to 2.0 V is normally required for commercial electrolyzers [13,16]. The open-circuit photo-voltages (V_{oc}) of commercial single-junction PV devices such as monocrystalline silicon (c-Si), gallium arsenide (GaAs), cadmium telluride (CdTe), and copper indium gallium selenide (CIGS) are generally less than 1 V [13,17,18]. Consequently, to obtain a high photo-voltage, single-cells are connected together in series [13,18]. However, this results in high commercial production-costs owing to the large quantity of materials used. To fulfil the high voltage requirement, some researches have focused on multi-junction cell configurations such as III-V triple-junction solar cells [7,19] or CIGS tandem solar cells [20]. However, the high trade-prices of these materials limits the practical application of these devices [21,22].

Consequently, with the aim of creating a high-efficiency, inexpensive PV-EWS system, we propose an innovative silicon-based tandem cell configuration. This system incorporates a two-terminal integration of a hydrogenated amorphous silicon germanium (a-SiGe:H) top cell and a monocrystalline silicon heterojunction (SHJ) bottom cell,

as shown in Fig. 1. Other researchers have proposed similar low-price silicon-based multi-junction photovoltaic configurations for PV-EWS applications, including hydrogenated amorphous silicon (a-Si:H)/microcrystalline silicon ($\mu\text{c-Si:H}$) tandem structure solar cells [23], a-Si:H/a-Si:H/ $\mu\text{c-Si:H}$ triple-junction solar cells, a-Si:H/ $\mu\text{c-Si:H}$ / $\mu\text{c-Si:H}$ triple-junction solar cells, a-Si:H/a-Si:H/ $\mu\text{c-Si:H}$ / $\mu\text{c-Si:H}$ quadruple junction solar cells [24], and a-Si:H/ $\mu\text{c-Si:H}$ /c-Si triple-junction solar cells [25]. For multi-junction configurations, the total photo-voltage of the solar cells is the approximate sum of each sub-cell photo-voltage, while the photo-current of the junctions essentially depends on that of the a-Si:H top cell [26]. The $\mu\text{c-Si:H}$ thin film solar cells suffer from a low V_{oc} (around 0.55 V), while a-Si:H cells suffer from a low J_{sc} [17]. In addition, triple or quadruple junctions require complex manufacturing technologies. Herein, we combined the advantages of the a-SiGe:H thin film top cell, such as the provision of a higher J_{sc} than that of an a-Si:H device [27–29] owing to the tuneable band-gap of the absorption layer, with the advantages of the SHJ bottom cell, such as high V_{oc} (approximately > 0.7 V) owing to efficient interface passivation. A two-terminal integrated configuration with a high V_{oc} and J_{sc} was thereby created. However, Ge-alloys can lower the band-gap of the absorption layer. They are also generally accompanied by more defects and a band-offset at the interfaces, thus impairing the V_{oc} of the fabricated device. To optimise the conversion performance of the a-SiGe:H top cell, we used band-gap engineering technology in conjunction with the a-SiGe:H absorption layer to control the output-cell parameters. The proposed tandem cell exhibits a high conversion performance of 16.1%, with a large enough V_{oc} (> 1.5 V) to permit stand-alone water electrolysis, and an estimated STH efficiency of 13.1%.

2. Experiment

We employed a plasma-enhanced chemical vapor deposition (PECVD) system to fabricate the PV device used in this study. Silane (SiH_4), hydrogen (H_2), and germane (GeH_4) were used as precursor gases for a-SiGe:H layer deposition. Single a-SiGe:H layers 300 nm in thickness were prepared on eagle glass and bare wafers under various $[\text{GeH}_4]/[\text{SiH}_4]$ gas ratios in the range of 0.1–0.26 and a constant $[\text{H}_2]/[\text{SiH}_4]$ gas ratio of 5. Optical properties such as the absorption coefficient (α) and the optical band-gap of these single-layers were determined from their ellipsometry spectra measurements obtained using the VASE J. A. Woollam system. The film thickness was determined from the fitting the ellipsometry data obtained using the Cauchy model in the wavelength range of 600–1700 nm. The micro-structural parameters of the films were calculated from their FTIR spectra (not shown here) as: $I_{2100}/(I_{2000} + I_{2100})$, where I_{2100} and I_{2000} are the integrated

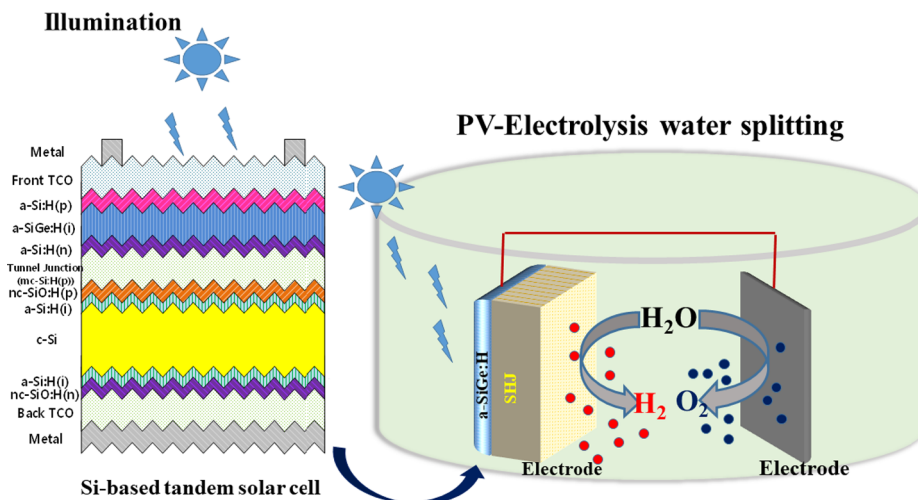


Fig. 1. Schematic of the photovoltaic-electrolysis water splitting system using an a-SiGe/SHJ tandem solar cell as the source of electricity.

absorption intensities of the peaks at wavenumbers of 2100 and 2000 cm^{-1} , respectively. The band-gap engineering technologies of the single-junction a-SiGe:H thin film solar cells were implemented by altering the $[\text{GeH}_4]/[\text{SiH}_4]$ gas ratio to 0.14, 0.18 and 0.22 during the deposition of the a-SiGe:H absorption layer, without disrupting the plasma source. The integrated a-SiGe:H/SHJ tandem configuration, as shown in Fig. 1, was implemented by directly depositing the a-SiGe:H top cell on the SHJ solar cells. The cells were characterised by J-V curves in dark and illuminated conditions using a standard illumination source at a one-sun illumination (AM1.5) and a power density of 100 mW/cm^2 . The QEX7 system (PV Measurement Inc.) was used to determine the external quantum efficiencies (EQEs) of all cells.

3. Results and discussion

Low-cost thin film a-Si:H has been used widely as the top sub-cell in Si-based multi-junction cell structures [30]. However, these cells suffer from low electrical current densities owing to the high band-gap (ranging from 1.7 to 1.8 eV) of the a-Si:H absorption layer, which allows them to effectively absorb sunlight only at short wavelengths below 700 nm. Improving the light-absorption at longer wavelengths—i.e. further diminishing the band-gap of the absorption layer—can further enhance the current density of the a-Si:H top cell and thereby improve the current density of silicon tandem solar cells [30,31]. The inherent band-gap of a-Si:H can be varied by 1.3 to 1.8 eV by alloying it with germanium (Ge) [32]. Fig. 2 shows the Tauc optical gaps and micro-structural parameters of a-SiGe:H absorption layers as a function of the Ge content. The band-gap of the a-SiGe:H absorption layers diminished from 1.7 to 1.5 eV with an increase in the Ge content, denoted by an increase in the $[\text{GeH}_4]/[\text{SiH}_4]$ gas ratio from 0.1 to 0.26. In addition, Fig. 2b shows a gradual increase in the micro-structural parameters with an increase in the gas ratio, i.e. an increase in the defect densities. This indicates that alloying with Ge not only diminishes the band-gap of the a-Si:H material, but also increases its defect density. The latter can cause a significant decrease in the V_{oc} and fill factor (FF), which in turn affects the total conversion performance [32]. Some reports have proposed that controlling the Ge content—i.e. rearranging band-gaps, known as band-gap engineering or band-gap grading techniques—throughout the thickness of the a-SiGe:H absorption layer can limit defect densities and promote carrier transportation and collection, thereby enhancing the a-SiGe:H cell efficiency [28,32–34].

We experimented using various band-gap engineering techniques on single-junction a-SiGe:H solar cells, as shown in Fig. 3, to determine the optimal technique for creating high-efficiency solar cells. In Fig. 3, the horizontal and vertical orientations denote the thickness and optical

band-gap of the layers, respectively. In cell A, which did not undergo band-gap engineering, a $[\text{GeH}_4]/[\text{SiH}_4]$ gas ratio of 0.22 was maintained during the absorption layer deposition, which resulted in an absorber band-gap of 1.58 eV. In cells B and C, the band-gap of the absorption layer was graded into five steps, while three steps were used in cells D and E. The $[\text{GeH}_4]/[\text{SiH}_4]$ gas ratio was instantly altered to values of 0.14, 0.18, and 0.22, corresponding to 1.68, 1.63, and 1.58 eV band-gaps, respectively. The thicknesses and band-gaps of each of step are illustrated in detail in Fig. 3. Fig. 4a and 4b show the current density-voltage (J-V) curves and EQEs, respectively, of single-junction a-SiGe:H cells with various band-gap configurations of the a-SiGe:H absorption layer. Cell parameters such V_{oc} , J_{sc} , FF, and efficiency (E_{ff}) are summarised in Table 1.

The band-gap engineering techniques, as shown in Fig. 3, caused an essential trade-off between the cell parameters. Researchers have applied various band-gap grading or profiling techniques to improve the conversion performance of a-SiGe:H thin film solar cells [27,29,33–35]. However, to date, a proper explanation for these techniques has not yet been obtained. As indicated in Fig. 2b, an increased Ge content can lower the band-gap of the a-SiGe:H absorption layer, thereby enhancing sunlight absorption at longer wavelengths [36]. As shown in Fig. 4b, the EQE at wavelengths greater than 660 nm of the reference-cell A, which did not undergo band-gap engineering, was higher than that of the other cells that underwent band-gap engineering. This results in a high J_{sc} of cell A, but low FF, possibly due to the high defect densities in this cell. The band-gap engineering applied in cells B to E that utilized wider band-gap layers of 1.68 eV and 1.63 eV can slightly enhance their EQEs for short wavelengths below 500 nm when compared with that of cell A. A narrow-gap a-SiGe:H layer distributed near the p/i interface, as shown in cells A and D, can possibly reduce the V_{oc} . Hsu et al. demonstrated that a narrow-gap a-SiGe:H at the p/i interface can cause a substantial band-offset between the high-gap p-doped layer and the intrinsic a-SiGe:H layer [37], thereby adversely affecting the internal electrical field as well as the carrier extraction [38,39]. Moreover, increased defect density due to the incorporation of a high Ge content can cause carrier collection losses [40], and negatively affect the V_{oc} [27,30]. A high band-gap layer located near the p/i interface, as shown in cells B, C, and E, can diminish interface states and improve the V_{oc} [33,35,39]. The band-gap engineering technique shown in cell D considerably enhanced the FF and J_{sc} leading to a high efficiency of 10.5%. Guha et al. [41] and Zimmer et al. [42] compared the different band-gap profiling techniques and noticed a similar trend, but a clear understanding of these techniques is still absent. The band-gap engineering configuration in cell D can considerably reduce the recombination rate and enhance the internal electric field, which results

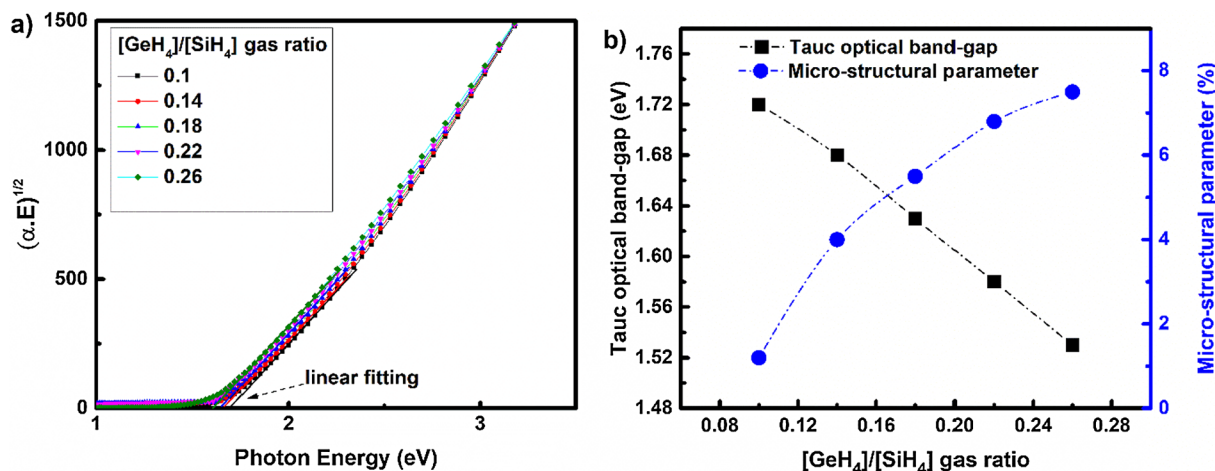


Fig. 2. (a) Plot of $(\alpha \cdot E)^{1/2}$ versus photon energy for the determination of the optical band-gap, and (b) the optical band-gap and micro-structural parameter as a function of the $[\text{GeH}_4]/[\text{SiH}_4]$ gas ratio.

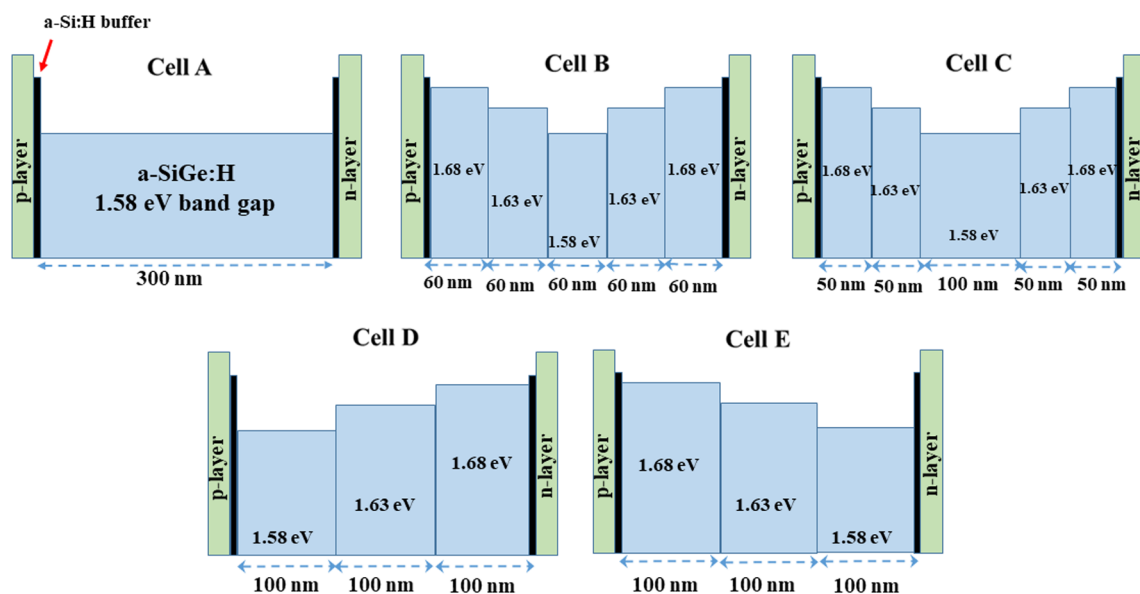


Fig. 3. Schematic of the single-junction a-SiGe:H solar cells with various band-gap engineering technologies used for the absorption layers.

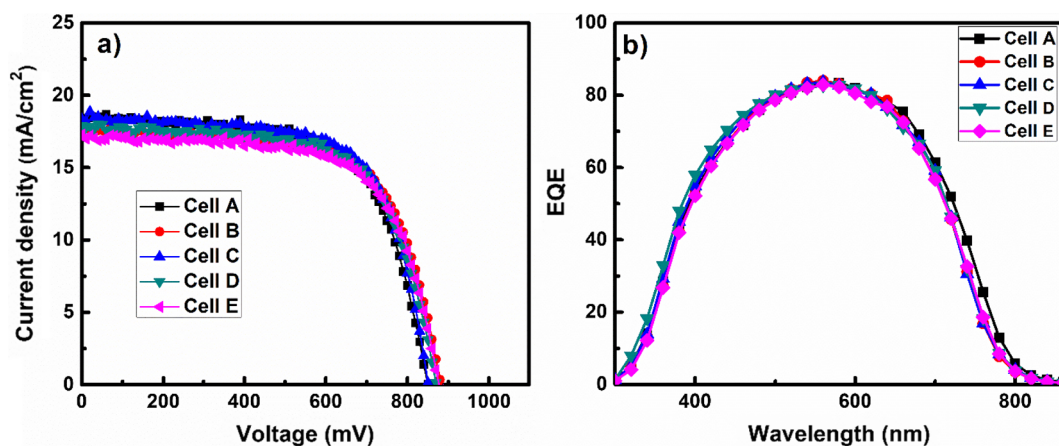


Fig. 4. (a) J-V curves and (b) EQE of single-junction a-SiGe:H solar cells with various band-gap engineering techniques.

Table 1
Single-junction a-SiGe:H cell parameters.

a-SiGe:H top cells	V_{oc} (V)	J_{sc} (mA/cm ²)	FF (%)	E_{ff} (%)	n	J_0 (mA/cm ²)
A	0.84	18.3	64	9.8	1.68	3.6×10^{-8}
B	0.88	17.2	66	9.9	1.51	2.5×10^{-9}
C	0.87	17.5	68	10.3	1.52	2.7×10^{-9}
D	0.85	18.0	68	10.4	1.59	8.6×10^{-9}
E	0.87	17.8	66	10.2	1.57	4.3×10^{-9}

in high FF and J_{sc} values [43]. In addition, we used the dark J-V characteristic measurements to calculate the inverse saturation current density (J_0) and diode ideal factor (n) [44], as shown in Fig. 5. The J_0 and n values of the cells are summarised in Table 1.

The J_0 and n values roughly indicate the carrier recombination/generation characteristic within the absorption layer. For example, a higher n value denotes a dominant bulk recombination within the intrinsic layer, while a lower J_0 value denotes the reduction of recombination losses, and results in a higher V_{oc} [44,45]. As shown in Table 1, the cells that underwent band-gap engineering (cells B to E) showed significantly lower J_0 and n values than the cell that did not (cell A). This demonstrates that band-gap engineering techniques substantially limit recombination losses within the narrow-gap a-SiGe:H

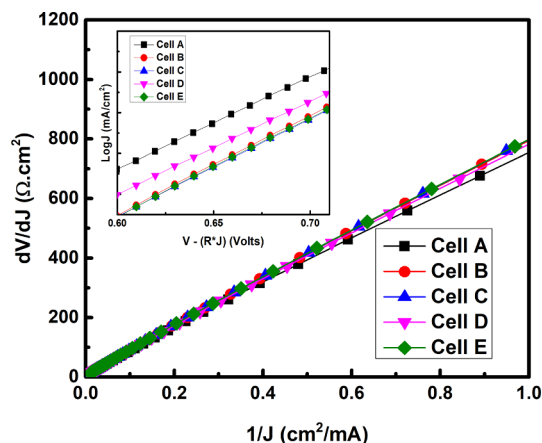


Fig. 5. Plot of dV/dJ versus $1/J$ from the dark I-V data of single-junction a-SiGe:H solar cells. Inset is the data of $\text{Log}J$ as a function of $[V - (R^*J)]$ wherein the slope of the linear fittings corresponds to q/nkT , and the intercepts are the J_0 values.

absorption layer and improve cell parameters. We applied the band-gap engineering techniques on an a-SiGe:H/SHJ tandem configuration to improve the solar cell efficiency. The illuminated J-V curves of the

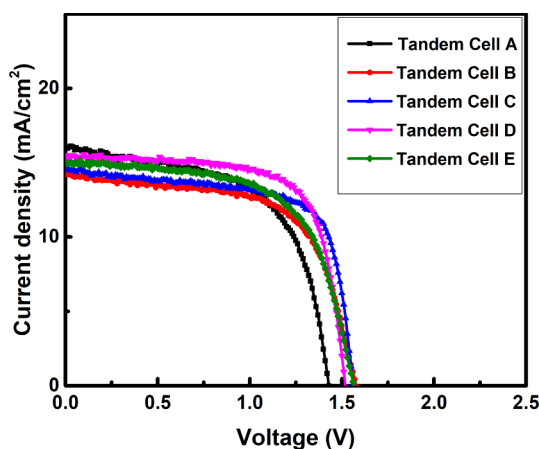


Fig. 6. J-V curves of the integrated a-SiGe:H/SHJ tandem solar cells with various band-gap engineering techniques used for the a-SiGe:H top cells.

Table 2
The a-SiGe:H/SHJ tandem cell parameters and estimated STH efficiency.

The tandem cells	V_{oc} (V)	J_{sc} (mA/cm ²)	FF (%)	E_{ff} (%)	STH efficiency (%)
A	1.40	16.0	60	13.44	11.8
B	1.57	14.3	62	13.91	10.89
C	1.56	14.5	69	15.6	12.3
D	1.51	15.5	69	16.14	13.14
E	1.55	15.0	63	14.64	11.61

tandem cells are shown in Fig. 6. The tandem cell parameter values are summarised in Table 2. The integrated a-SiGe:H/SHJ tandem configuration had a V_{oc} over 1.5 V, which fulfils one of the essential requirements for EWS applications. The tandem cell A without band-gap engineering of the top cell had low V_{oc} and FF values, which is probably due to the high defect densities in the absorption layer of the a-SiGe:H top cell. The band-gap engineering in the tandem cell D resulted in high J_{sc} and FF values, which increased the tandem efficiency to 16.14%. Notably, the cell parameter variation trends of the tandem structures, as shown in Table 2, with the different top-cell band-gap engineering technologies corresponded to those of the single-junction a-SiGe:H cells, as shown in Table 1. This indicates that band-gap engineering of the top cell can control the trade-off relationships between the cell parameters and thus improve the efficiency of the tandem cell structures.

Having obtained improved the performance of the PV tandem device, we now estimate the matching-capacity of the PV generator and the electrolysis system. The direct monolithic combination of the PV-EWS, as shown in Fig. 1, was performed to limit the need for intervening electronics and thereby reduce the manufacturing costs [46,47]. Other coupling options such as usage of a DC/DC converter with a maximum power point tracker have also been suggested [48,49]. While configurations with the DC/DC converter maintain high stability and efficiency, they also increase the cost and complexity [47]. In an integrated PV-EWS system (Fig. 1), the current generated by the electrolysis system is primarily limited by the current of the PV device, while the PV device must generate a voltage greater than 1.5 V to induce the electrolysis reaction. Therefore, the PV-EWS performance depends primarily on the performance of the PV solar cells. The STH conversion efficiency (η) can be estimated typically via the energy efficiency of electrolysis coupled with the PV device efficiency (PCE) [15]. The energy efficiency of electrolysis is defined as the ratio of the reversible potential of the water decomposition (1.23 V) to the applied operation voltage for electrolysis. In an ideal case, the electrolyser can operate under the V_{oc} conditions of an integrated PV device; as a result,

$\eta = (1.23 \text{ V})(\text{PCE})/V_{oc}$. Using this definition, we estimated the STH conversion efficiency, as shown in Table 2, assuming that the tandem cells operated at ideal conditions with maximum output conversion performances. This implies that the current of the PEC system almost corresponds to the current density generated by the PV devices. The η values are summarised in Table 2. The results show that a high STH efficiency of 13.1% was achieved by cell D, which possesses a high PCE of 16.1%. It appears that in the process of determining η , the energy efficiency ($1.23/V_{oc}$) exhibits an efficiency loss when V_{oc} is increased, and the PCE provides an efficiency compensation factor. Compared with the V_{oc} of tandem cell D, a high V_{oc} over 1.55 V for the tandem cells B, C, and E can result in higher efficiency losses for STH production. A high PCE is required to compensate for these losses to achieve a high STH efficiency; however, the lower FF or J_{sc} values of tandem cell B, C, and E result in a lower PCE than that of cell D. In tandem cell A, although the efficiency losses are likely lower than that of cell D owing to a lower V_{oc} , as shown in Table 2, low V_{oc} and FF values result in a significantly low PCE; as a result, a lower STH efficiency is observed. The high STH efficiency of cell D can stem from the sufficiently low V_{oc} of 1.51 V which limits efficiency losses and permits a high PCE of 16.1%. It can be concluded that the band-gap engineering in cell D enhances the efficiency of the tandem structure and improves the PV-EWS system performance.

For practical applications, the drawback of the PV-EWS system is its high commercial cost. The c-Si solar cell is the most popular commercial material and accounts for approximately 60% of the PV market demand. Producing electricity at competitive prices would require an increase in conversion performance while using a very thin silicon wafer [50]. The maximum laboratory cell efficiency reported thus far is 26.7% [17]. For PV-EWS applications, as single-junction silicon solar cells are only capable of low V_{oc} values of around 0.55 V, two or three of these single cells must be connected in series to fulfil the potential requirement for water electrolysis, which further increases the manufacturing cost [51]. While thin film Si-based multi-junction PV devices are a potential option for low-cost PV-EWS systems, their low stabilities and efficiencies remain inadequate. Consequently, the integration of low-cost thin film technology with high-stability SHJ devices, as proposed in this work, presents enormous potential for low-cost and high-performance PV-EWS systems.

4. Conclusion

In this study, we demonstrated the potential of integrated a-SiGe:H/SHJ tandem solar cells for use in PV-EWS systems owing to their high output voltage. We optimised the conversion performance of the tandem cells using a band-gap engineering process for the a-SiGe:H top cells. The band-gap engineering technique used in cell D decreased the defect densities in the absorption layer and enhanced the internal electric field, thereby improving carrier transportation and collection. Consequently, a high tandem efficiency of 16.1% with a high V_{oc} of greater than 1.5 V was obtained. The direct coupling of this tandem configuration with EWS systems can provide an idealised STH conversion performance of 13.1%. Furthermore, we believe that the a-SiGe:H/SHJ tandem configuration can achieve a lower manufacturing cost than in the case of multiple c-Si single-junction solar cells connected in series.

Declaration of Competing Interest

The authors declare that they have no known competing financial interests or personal relationships that could have appeared to influence the work reported in this paper.

Acknowledgements

This work was supported by the New & Renewable Energy Core Technology Program of the Korea Institute of Energy Technology Evaluation and Planning (KETEP), and granted financial resource from the Ministry of Trade, Industry & Energy, Republic of Korea (No. 20183010014270 and No. 20193010014850).

References

- [1] T.R. Cook, D.K. Dogutan, S.Y. Reece, Y. Surendranath, T.S. Teets, D.G. Nocera, Solar energy supply and storage for the legacy and nonlegacy worlds, *Chem. Rev.* 110 (2010) 6474–6502.
- [2] F. Zhang, P. Zhao, M. Niu, J. Maddy, The survey of key technologies in hydrogen energy storage, *Int. J. Hydrogen Energy* 41 (2016) 14535–14552.
- [3] A. Fujishima, K. Honda, *Nature* 238 (1972) 37.
- [4] F.E. Osterloh, Inorganic nanostructures for photoelectrochemical and photocatalytic water splitting, *Chem. Soc. Rev.* 42 (2013) 2294–2320.
- [5] H.M. Chen, C.K. Chen, R.S. Liu, L. Zhang, J. Zhang, D.P. Wilkinson, Nano-architecture and material designs for water splitting photoelectrodes, *Chem. Soc. Rev.* 41 (2012) 5654–5671.
- [6] Z. Li, W. Luo, M. Zhang, J. Feng, Z. Zou, Photoelectrochemical cells for solar hydrogen production: current state of promising photoelectrodes, methods to improve their properties, and outlook, *Energy Environ. Sci.* 6 (2013) 347–370.
- [7] S. Okamoto, M. Deguchi, S. Yotsuhashi, Modulated III–V triple-junction solar cell wireless device for efficient water splitting, *J. Phys. Chem. C* 121 (2017) 1393–1398.
- [8] S. Koumi Ngoh, D. Njomo, An overview of hydrogen gas production from solar energy, *Renew. Sustain. Energy Rev.* 16 (2012) 6782–6792.
- [9] K. Maeda, Z-scheme water splitting using two different semiconductor photocatalysts, *ACS Catal.* 3 (2013) 1486–1503.
- [10] S. Esiner, R.E.M. Willems, A. Furlan, W. Li, M.M. Wienk, R.A.J. Janssen, Photoelectrochemical water splitting in an organic artificial leaf, *J. Mater. Chem. A* 3 (2015) 23936–23945.
- [11] X. Elias, Q. Liu, C. Gimbert-Suriñach, R. Matheu, P. Mantilla-Perez, A. Martinez-Otero, et al., Neutral water splitting catalysis with a high FF triple junction polymer cell, *ACS Catal.* 6 (2016) 3310–3316.
- [12] J. Chen, D. Yang, D. Song, J. Jiang, A. Ma, M.Z. Hu, et al., Recent progress in enhancing solar-to-hydrogen efficiency, *J. Power Sour.* 280 (2015) 649–666.
- [13] J. Luo, J.H. Im, M.T. Mayer, M. Schreier, M.K. Nazeeruddin, N.-G. Park, S.D. Tilley, H.J. Fan, M. Gratzel, Water photolysis at 12% efficiency via perovskite photovoltaics and earth-abundant catalysts, *Science* 345 (2014) 1593–1596.
- [14] J. Qi, W. Zhang, R. Cao, Solar-to-hydrogen energy conversion based on water splitting, *Adv. Energy Mater.* 8 (2018) 1701620.
- [15] O. Khaselev, A. Bansal, J.A. Turner, High efficiency integrated multijunction photovoltaic electrolysis systems for hydrogen production, *Int. J. Hydrogen Energy* 26 (2001) 127–132.
- [16] H. Dotan, N. Mathews, T. Hisatomi, M. Gratzel, A. Rothschild, On the solar to hydrogen conversion efficiency of photoelectrodes for water splitting, *J. Phys. Chem. Lett.* 5 (2014) 3330–3334.
- [17] M.A. Green, E.D. Dunlop, D.H. Levi, J. Hohl-Ebinger, M. Yoshita, A.W.Y. Ho-Baillie, Solar cell efficiency tables (version 54), *Prog. Photovoltaics Res. Appl.* 27 (2019) 565–575.
- [18] J.W. Ager, M.R. Shaner, K.A. Walczak, I.D. Sharp, S. Ardo, Experimental demonstrations of spontaneous, solar-driven photoelectrochemical water splitting, *Energy Environ. Sci.* 8 (2015) 2811–2824.
- [19] E. Verlage, S. Hu, R. Liu, R.J.R. Jones, K. Sun, C. Xiang, et al., A monolithically integrated, intrinsically safe, 10% efficient, solar-driven water-splitting system based on active, stable earth-abundant electrocatalysts in conjunction with tandem III–V light absorbers protected by amorphous TiO₂ films, *Energy Environ. Sci.* 8 (2015) 3166–3172.
- [20] T.J. Jacobsson, V. Fjällström, M. Sahlberg, M. Edoff, T. Edvinsson, A monolithic device for solar water splitting based on series interconnected thin film absorbers reaching over 10% solar-to-hydrogen efficiency, *Energy Environ. Sci.* 6 (2013) 3676.
- [21] S. Essig, C. Allebé, T. Remo, J.F. Geisz, M.A. Steiner, K. Horowitz, et al., Raising the one-sun conversion efficiency of III–V/Si solar cells to 32.8% for two junctions and 35.9% for three junctions, *Nature Energy* 2 (2017).
- [22] R. Cariou, J. Benick, F. Feldmann, O. Höhn, H. Hauser, P. Beutel, et al., III–V-on-silicon solar cells reaching 33% photoconversion efficiency in two-terminal configuration, *Nat. Energy* 3 (2018) 326–333.
- [23] F. Urbain, V. Smirnov, J.-P. Becker, U. Rau, F. Finger, J. Ziegler, et al., a-Si:H/ μ c-Si:H tandem junction based photocathodes with high open-circuit voltage for efficient hydrogen production, *J. Mater. Res.* 29 (2014) 2605–2614.
- [24] F. Urbain, V. Smirnov, J.-P. Becker, A. Lambertz, F. Yang, J. Ziegler, et al., Multijunction Si photocathodes with tunable photovoltages from 2.0 V to 2.8 V for light induced water splitting, *Energy Environ. Sci.* 9 (2016) 145–154.
- [25] S. Kirner, H. Sarajan, A. Azarpira, T. Schedel-Niedrig, B. Stannowski, B. Rech, et al., Wafer surface tuning for a-Si:H/ μ c-Si:H/c-Si triple junction solar cells for application in water splitting, *Energy Procedia* 102 (2016) 126–135.
- [26] J. Park, V.A. Dao, S. Kim, D.P. Pham, S. Kim, A.H.T. Le, et al., High efficiency inorganic/inorganic amorphous silicon/heterojunction silicon tandem solar cells, *Sci. Rep.* 8 (2018) 15386.
- [27] D.P. Pham, S. Kim, A.H. Tuan Le, J. Park, J. Yi, Diminished band discontinuity at the p/i interface of narrow-gap a-SiGe: H solar cell by hydrogenated amorphous silicon oxide buffer layer, *J. Alloy. Compd.* 762 (2018) 616–620.
- [28] D.P. Pham, S. Kim, J. Park, A.T. Le, J. Cho, J. Jung, et al., Silicon germanium active layer with graded band gap and μ c-Si: H buffer layer for high efficiency thin film solar cells, *Mater. Sci. Semicond. Process.* 56 (2016) 183–188.
- [29] D.P. Pham, S. Kim, J. Park, A.H.T. Le, J. Cho, J. Yi, Improvement in carrier collection at the i/n interface of graded narrow-gap hydrogenated amorphous silicon germanium solar cells, *J. Alloy. Compd.* 724 (2017) 400–405.
- [30] F. Meillaud, M. Boccard, G. Bugnon, M. Despeisse, S. Hänni, F.J. Haug, et al., Recent advances and remaining challenges in thin-film silicon photovoltaic technology, *Mater. Today* 18 (2015) 378–384.
- [31] T.P. White, N.N. Lal, K.R. Catchpole, Tandem solar cells based on high-efficiency c-Si bottom cells: top cell requirements for > 30% efficiency, *IEEE J. Photovoltaics* 4 (2014) 208–214.
- [32] B. Liu, L. Bai, X. Zhang, C. Wei, Q. Huang, J. Sun, et al., Fill factor improvement in PIN type hydrogenated amorphous silicon germanium thin film solar cells: omnipotent n-type μ c-SiO_x: H layer, *Sol. Energy Mater. Sol. Cells* 140 (2015) 450–456.
- [33] J.-W. Chung, J.W. Park, Y.J. Lee, S.-W. Ahn, H.-M. Lee, O.O. Park, Graded layer modification for high efficiency hydrogenated amorphous silicon-germanium solar cells, *Jpn. J. Appl. Phys.* 51 (2012) 10NB6.
- [34] R.J. Zambrano, F.A. Rubinelli, W.M. Arnoldbik, J.K. Rath, R.E.I. Schropp, Computer-aided band gap engineering and experimental verification of amorphous silicon-germanium solar cells, *Sol. Energy Mater. Sol. Cells* 81 (2004) 73–86.
- [35] R.J. Zambrano, F.A. Rubinelli, J.K. Rath, R.E.I. Schropp, Improvement in the spectral response at long wavelength of a-SiGe: H solar cells by exponential band gap design of the i-layer, *J. Non-Cryst. Solids* 299–302 (2002) 1131–1135.
- [36] P. Agarwal, H. Povolny, S. Han, X. Deng, Study of a-SiGe: H films and n-i-p devices used in high efficiency triple junction solar cells, *J. Non-Cryst. Solids* 299–302 (2002) 1213–1218.
- [37] H.-J. Hsu, C.-H. Hsu, C.-C. Tsai, Improvement of a-Si1-xGex: H single-junction thin-film solar cell performance by bandgap profiling techniques, *J. Non-Cryst. Solids* 358 (2012) 2277–2280.
- [38] D. Lundszen, F. Finger, H. Wagner, A-Si: H buffer in a-SiGe: H solar cells, *Solar Energy Mater. Solar Cells* 74 (2002) 365–372.
- [39] D. Lundszen, F. Finger, H. Wagner, Band-gap profiling in amorphous silicon-germanium solar cells, *Appl. Phys. Lett.* 80 (2002) 1655–1657.
- [40] D.P. Pham, S. Kim, J. Park, J. Cho, H. Kim, A.H.T. Le, et al., Role of a-Si: H buffer layer at the p/i interface and band gap profiling of the absorption layer on enhancing cell parameters in hydrogenated amorphous silicon germanium solar cells, *Optik* 136 (2017) 507–512.
- [41] S. Guha, J. Yang, A. Pawlikiewicz, T. Glatfelter, R. Ross, S.R. Ovshinsky, Band-gap profiling for improving the efficiency of amorphous silicon alloy solar cells, *Appl. Phys. Lett.* 54 (1989) 2330–2332.
- [42] J. Zimmer, H. Stiebig, H. Wagner, a-SiGe: H based solar cells with graded absorption layer, *J. Appl. Phys.* 84 (1998) 611–617.
- [43] D.P. Pham, S. Kim, J. Park, A.H. Tuan Le, J. Cho, J. Jung, et al., Reduction in photocurrent loss and improvement in performance of single junction solar cell due to multistep grading of hydrogenated amorphous silicon germanium active layer, *Silicon* 10 (2017) 759–767.
- [44] S.S. Hegedus, Current Voltage analysis of a-Si and a-SiGe solar cell including voltage dependent photocurrent collection, *Prog. Photovoltaics Res. Appl.* 5 (1997) 151–168.
- [45] S.S. Hegedus, W.N. Shafarman, Thin-film solar cells: device measurements and analysis, *Prog. Photovoltaics Res. Appl.* 12 (2004) 155–176.
- [46] R.E. Clarke, S. Giddey, F.T. Ciacchi, S.P.S. Badwal, B. Paul, J. Andrews, Direct coupling of an electrolyser to a solar PV system for generating hydrogen, *Int. J. Hydrogen Energy* 34 (2009) 2531–2542.
- [47] O. Atlam, F. Barbir, D. Bezmalinovic, A method for optimal sizing of an electrolyzer directly connected to a PV module, *Int. J. Hydrogen Energy* 36 (2011) 7012–7018.
- [48] H. Solmecke, O. Just, D. Hackstein, Comparison of solar hydrogen storage systems with and without power-electronic DC-DC-converters, *Renew. Energy* 19 (2000) 333–338.
- [49] R. Garciaivalverde, C. Miguel, R. Martinezbejar, A. Urbina, Optimized photovoltaic generator–water electrolyser coupling through a controlled DC-DC converter, *Int. J. Hydrogen Energy* 33 (2008) 5352–5362.
- [50] J. Haschke, O. Dupré, M. Boccard, C. Ballif, Silicon heterojunction solar cells: Recent technological development and practical aspects - from lab to industry, *Sol. Energy Mater. Sol. Cells* 187 (2018) 140–153.
- [51] A.J. Bard, M.A. Fox, Artificial photosynthesis: solar splitting of water to hydrogen and oxygen, *Acc. Chem. Res.* 28 (1995) 141–145.